Evidence for Bose-Einstein condensation of excitons in Cu_2O

D. W. Snoke and J. P. Wolfe
Physics Department and Materials Research Laboratory, University of Illinois at Urbana-Champaign, 1110 West Green Street, Urbana, Illinois 61801

A. Mysyrowicz
Laboratoire d'Optique Appliquée, École Nationale Supérieure de Techniques Avancées, Ecole Polytechnique, Palaiseau F-91120, France and Groupe de Physique des Solides, Université de Paris 7, Paris, France
(Received 22 January 1990)

Pulsed-laser excitation of naturally grown crystals of Cu_2O produces a dense gas of excitons, which exhibits Bose-Einstein quantum statistics. Both orthoexcitons and paraexcitons, split by a 12-meV electron-hole exchange energy, are formed. At high excitation levels, the time-resolved luminescence of orthoexcitons yields a density-temperature relation that follows the phase boundary for Bose-Einstein condensation, $n = CT^{3/2}$, but no striking evidence for a condensed fraction is observed. We have now measured the time-resolved spectrum of the lower-lying paraexcitons whose luminescence is 1500 times weaker than the orthoexciton luminescence. At intermediate power levels, the paraexciton distribution is more degenerate than the orthoexcitons. The relative intensities of the two species indicate that at high excitation levels the paraexciton density exceeds the critical density for condensation. At these high densities the paraexciton spectrum develops a structure that cannot be explained in terms of the thermalized Bose-Einstein distribution. Time-resolved spatial measurements of the luminescence indicate a rapid nondiffusive expansion of the gas at supersonic velocities that approach the expected ballistic velocities of the excitons. The rapid transport and the concurrent changes in the spectral distribution of paraexcitons may be the first observation of excitonic Bose-Einstein condensation and superfluidity.

I. INTRODUCTION

Due to its boson nature and light mass, the exciton (bound electron-hole pair) produced by photoexcitation of a semiconductor at low temperatures is a natural candidate for observing Bose-Einstein condensation.[1-3] While this fact has been recognized for some time, a clear demonstration of Bose-Einstein condensation (BEC) of excitons has not yet appeared. It has been demonstrated, however, that for semiconductors with sufficiently long excitonic recombination times, excitons can form a nearly ideal boson gas that departs from classical statistics and manifests Bose-Einstein statistics. Bose-Einstein statistics are not normally observed in the indirect-gap semiconductors silicon and germanium because at zero stress the attractive forces between excitons in these crystals result in condensation of the gas into a fermionic electron-hole liquid. Nevertheless, by application of appropriate stress, the liquid binding in Ge can be reduced, and evidence has been reported for mildly quantum statistics of excitons.[4] Also, direct-gap CuCl is found to support a dense gas of strongly bound biexcitons which at high density appear to exhibit Bose-Einstein statistics.[5]

The best candidate for observing a thermodynamic condensation of excitons appears to be Cu_2O,[6,7] which has a parity-forbidden direct gap—implying relatively long excitonic lifetimes[8]—and a band structure which results in repulsive forces between excitons.[9] Indeed, at high exciton densities, no biexcitons or electron-hole liquid have been observed for this crystal.

In a previous publication,[7] we reported the creation of a highly degenerate orthoexciton gas in Cu_2O, displaying an average density that is within a factor of 2 of the BEC critical density. These results were obtained by time- and space-resolved spectroscopy of the recombination luminescence, following surface excitation by an intense 10-ns laser pulse. During and after the laser pulse, the exciton density rises and falls due to the competing generation, recombination, and expansion processes. From the earliest measurement times the gas exhibits a well defined, but time-dependent, temperature. The most interesting observation is that, for over an order of magnitude in density, the gas temperature increases and falls in such a way as to keep the gas paralleling the BEC phase boundary, $n = CT^{3/2}$. Nevertheless, we reported no dramatic evidence for a condensed phase; e.g., a sharp spike in the luminescence spectrum at zero kinetic energy.

In the present paper, we report new analyses and results that indicate an actual Bose-Einstein condensation of the excitonic gas in Cu_2O. First, we have analyzed the time-resolved spectra of the orthoexcitons taking into account the spatial inhomogeneities which must be present in the gas. We conclude that the orthoexciton gas indeed has a maximum density about equal to the BEC critical density. At high densities the spectra exhibit a low-energy tail which indicates frequent exciton-exciton collisions and possibly interactions with a condensate.

Secondly, we have succeeded in measuring the time-resolved photoluminescence of paraexcitons. (The paraexcitons lie lower than the orthoexcitons by an exchange energy of 12 meV, and they have 1500 times weaker luminescence than the latter.) From the relative intensities, we conclude that the maximum density of paraexcitons is actually higher than the critical density for condensation. In addition, at moderate excitation levels, the paraexciton spectrum is significantly sharper than that of the orthoexcitons, indicating that the paraexciton gas is more degenerate than the orthoexciton gas. At the highest excitation levels a highly anomalous energy distribution is observed for the paraexcitons which we associate with condensation.

Finally, we have directly measured the spatial expansion of the excitonic gas and find that the expansion velocity is power dependent and, at the highest excitation-power densities, supersonic. The expansion rate is greater than that predicted by simple diffusion and may indicate superfluid transport of excitons.[10] The simultaneous appearance of all these spectral and spatial effects provides a compelling case for Bose-Einstein condensation.

Before describing these results, we mention some important aspects of the problem that are not directly considered here. First is the question of whether the excitons, treated as an ideal Bose gas, have sufficient time to condense into the ground state; that is, can they condense within the excitonic lifetime? After photoexcitation and the initial carrier relaxation by optical phonon emission, the excitons are formed with high kinetic energies. By computer simulation, we have determined how quickly the hot gas assumes a degenerate energy distribution.[11] These calculations suggest that a macroscopic occupation of the ground state is possible within the known excitonic lifetimes. Secondly, what is the source of the temperature rise in the excitonic gas at high density? It seems likely that the gas is heated in part by the Auger process, whereby one exciton recombines giving its recombination energy to another exciton, which ionizes into an energetic electron and hole.[12,13] A model calculation including phonon emission, Auger recombination, and orthoexciton-to-paraexciton conversion indeed shows a pronounced temperature rise in the gas at high density and will be reported in a subsequent paper. In the present paper we ignore these microscopic kinetic processes and simply use the photoluminescence to determine the density, temperature and volume of the excitonic gas.

II. EXPERIMENTAL PROCEDURE

In these experiments, a high-purity naturally grown crystal of Cu_2O is immersed in superfluid ^4He at 2 K and excited with Ar^+-laser light at wavelength 5145 Å, which has an absorption length of 1.6 μm in Cu_2O.[14] Figure 1 shows a level diagram for the excitation and relaxation processes in this experiment. The laser beam, focused to produce absorbed powers up to 10^7 W/cm^2 during 8-ns cavity-dumped pulses, produces electron-hole pairs with large kinetic energies ($h\nu - E_{gap} \sim 0.375$ eV), which

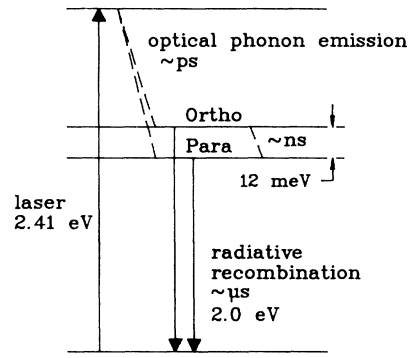

FIG. 1. Simplified level diagram for Cu_2O. The vertical axis is not drawn to scale.

thermalize by emission of phonons and pair into excitons on a subnanosecond timescale.[15] The exciton has binding energy of about 0.15 eV and a Bohr radius of about 7 Å.[16]

The recombination luminescence of the excitons is collected by a lens and focused onto the entrance slit of a 1-m spectrometer with 0.25 Å spectral resolution. By scanning the magnified image of the excitation spot across the entrance slit and a crossed slit, we can achieve 1-μm spatial resolution in two dimensions. We achieve 390-ps time resolution [full width at half maximum (FWHM), for a 100-ps mode-locked Ar^+-laser pulse] by focusing the exit slit of the spectrometer to a 100-μm spot on the photocathode of an RCA 31034A phototube and by using Tennelec constant-fraction discriminators and an Ortec time-to-pulse-height converter.

Both triply degenerate orthoexcitons ($^3\Gamma_5^+$) and singly degenerate paraexcitons ($^1\Gamma_2^+$) are formed by the excitation. Orthoexcitons, with exchange energy 12 meV above the paraexcitons,[17] can decay by conversion to paraexcitons and by radiative recombination. Both orthoexcitons and paraexcitons also decay nonradiatively via an Auger-like process, as discussed in the following. At the relevant gas densities of 10^{17} to 10^{19} cm^{-3}, the excitons collide with each other many times, so that quasiequilibrium temperatures and chemical potentials can be defined. At these densities, the exciton-exciton interaction time is estimated to be on the order of a few picoseconds or less, assuming hard-sphere scattering, whereas the measured orthoexciton lifetimes are of the order of one nanosecond. The luminescence spectra show a well-defined temperature at all observation times. Due to the rapid collision rate, the paraexcitons and orthoexcitons should have the same temperature at all observation times, but in general they have different quasiequilibrium chemical potentials, since the conversion time between species is slow. We discuss the relative orthoexciton and paraexciton densities in Sec. VI.

Even though the interaction time is short, the excitons are still expected to remain bosons in nature, i.e., fulfill the condition[1] $na^3 \ll 1$. For density as high as 10^{20} excitons/cm^3, $na^3 = 0.035$ for the excitonic Bohr radius, $a = 7$ Å.

The short absorption length of the 5145-Å laser light and the finite diffusion constant of the excitons have the

effect of inertially confining the excitons to a small volume. The characteristic exciton-cloud expansion speeds are on the order of the sound velocity, a few microns per nanosecond. On the nanosecond timescale of the laser pulse, the flat disk of excitons created at the surface simply does not have time to greatly increase its volume. Looking at very early times thus gives us the ability to see the gas at very high densities. At times after the laser pulse, most of the orthoexcitons will have converted to paraexcitons, which have microsecond lifetimes and diffuse deep into the crystal.[13,18]

Since the phonon-assisted recombination rates of the excitons do not depend on the exciton kinetic energy, the phonon-assisted luminescence spectra give the kinetic-energy distribution of the excitons directly. Quantum statistics for an ideal or weakly interacting gas of integral-spin particles predicts the Bose-Einstein distribution function, with the form

$$f(\epsilon,\alpha)=\frac{1}{e^{\epsilon+\alpha}-1}\ , \tag{1}$$

where $\epsilon \equiv E/k_B T$ with E the exciton kinetic energy, and $\alpha \equiv -\mu/k_B T$, with μ the chemical potential of the gas. For a uniform-density gas at temperature T, α is determined by the condition

$$N = g(m/2\pi h^2)^{3/2}(k_B T)^{3/2}\int f(\epsilon,\alpha)D(\epsilon)d\epsilon\ , \tag{2}$$

where N is the number of particles and $D(\epsilon)$ is the density of states, proportional to $VE^{1/2}$ for particles in a volume V at constant potential energy. In this equation m is the particle mass and g is the spin multiplicity. For $\alpha \gg 1$, the distribution f corresponds to a classical Maxwell-Boltzmann distribution, while for α less than 1, the distribution f departs continuously from its classical shape. In the limit of $\alpha=0$, the spectrum exhibits a sharp peak at $E=0$ corresponding to Bose condensation. Figure 2 shows the predicted energy distributions for three values of α. This logarithmic plot shows that although the distribution becomes much more peaked as the gas approaches condensation, the exponential decay of the high-energy tail depends only on the temperature. For this reason, the two fit parameters, α and T, are practically orthogonal.

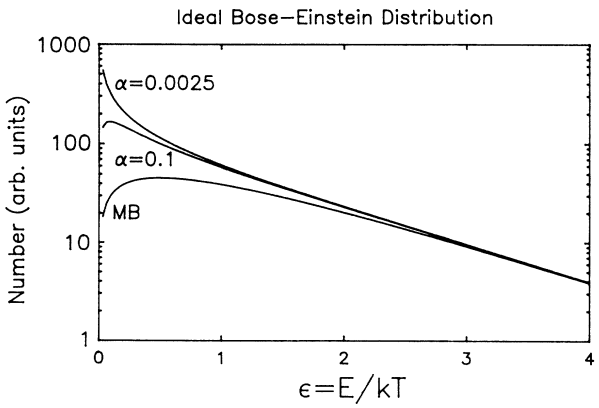

FIG. 2. The distribution $f(\epsilon,\alpha)D(\epsilon)$ for a Bose-Einstein gas, from Eq. (1) in the text, using a density of states proportional to $E^{1/2}$, for a three-dimensional gas at constant potential, for three values of $\alpha \equiv -\mu/k_B T$. Maxwell-Boltzmann (MB) corresponds to $\alpha > 4$. The intensities of the distributions at high energy have been set equal.

It is important to consider at this point how the existence of a condensate would manifest itself in the luminescence spectral, according to ideal Bose-Einstein statistics. It is apparent from Fig. 2 that the excited-state distribution exhibits a peak near zero kinetic energy that becomes sharper and sharper as α approaches zero. Thus, a separate peak associated with a condensate at $\epsilon=0$ cannot be resolved. Once the critical value $\alpha=0$ is reached,[19] the excited-state distribution can no longer increase. At higher densities, a condensate should manifest itself as an increase in the peak at $\epsilon=0$, causing the spectrum to become still sharper. The exact shape of the spectrum for the ideal Bose-Einstein condensate depends on the spectral resolution in the experiment as well as on any intrinsic spectral broadening in the gas. In principle, given the spectral broadening, the amount of condensate can be determined from the spectrum, even though no separate peak is resolved.

Of course, Eqs. (1) and (2) apply for a weakly interacting gas with a constant volume. In this system the gas volume is not constant, since excitons are free to diffuse into the crystal. If the gas is above the critical density for Bose condensation, possibly with superfluid expansion, it may not exhibit a spectral peak at zero kinetic energy but instead take on a finite average momentum. Also, at high enough densities, particle-particle interactions will cause an energy broadening of the ground state. Strong repulsive interactions in the gas will cause other effects, such as a phononlike behavior of the dispersion relation at low energy (see Sec. VI).

III. BOSE-EINSTEIN LINE SHAPE OF THE ORTHOEXCITON PHONON-ASSISTED LUMINESCENCE

Figure 3 shows the luminescence spectrum as a function of time for the case of high-power cavity-dumped Ar^+ laser excitation. Several of these spectra are plotted logarithmically in Fig. 4. The dashed lines are the best fits to the distribution $f(\epsilon,\alpha)D(\epsilon)$ given by Eq. (1). The logarithmic scale emphasizes the straight-line fit to the exponential high-energy tail. The most notable discrepancy between data and theory is the significant experimental intensity at $\epsilon<0$ (i.e., a "low-energy tail"). This tail can be accounted for by convolving $f(\epsilon,\alpha)D(\epsilon)$ with a Lorentzian spectral broadening on the order of 0.1 meV, shown as the open circles and discussed in Sec. IV. In each case, including the spectral broadening gives a fit to a much more degenerate distribution. Specifically, with broadening, the fits yield values of α in the range $0.001 < \alpha < 0.1$ for the orthoexcitons during and immediately after the excitation. For the spectral resolution used here, fits with $\alpha < 0.001$ are essentially indistinguishable from $\alpha=0$, with no condensate fraction added. The fit of Fig. 4(d) therefore corresponds to a density right at the critical value for condensation at $T=26$ K. We caution, however, that there is a significant uncertainty in

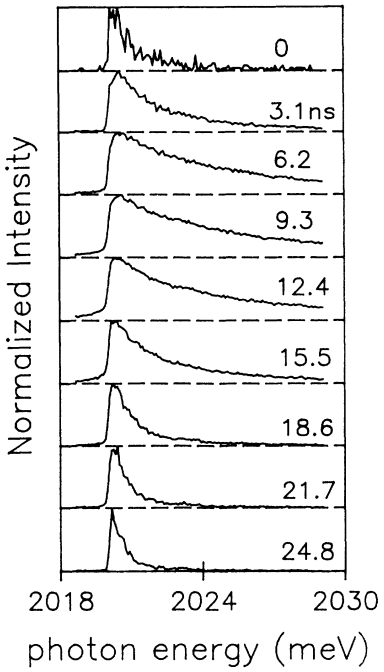

FIG. 3. Orthoexciton Γ_3^--phonon-assisted luminescence spectrum at various times during and after a 10-ns cavity-dumped Ar^+-laser pulse focused on the surface of a Cu_2O crystal immersed in liquid helium at 2 K. The peak of the pulse is at $t=9.3$ ns. The incident-laser-pulse energy is 0.3 μJ and spot diameter (FWHM) is roughly 10 μm, corresponding to a power density of roughly 4×10^7 W/cm^2. The spectra are plotted on a linear intensity scale and normalized to the same peak intensity.

these small values of α observed at late times because the fits to these narrower spectra are much more sensitive to the value chosen for the spectral broadening.

Under these surface-excitation conditions, the exciton gas actually exhibits a range of densities at any moment in time, so that it is not clear why a single chemical potential should describe the actual energy distribution. We show by modeling in Sec. IV that the α and T obtained from these fits actually give a reasonable approximation of these parameters for the region of highest exciton density.

As reported in Ref. 12, the exciton-gas temperature ranges up to 70 K during the cavity-dumped pulse. The *lattice* temperature, however, remains below 15 K, as indicated by the almost negligible band-gap shift of the spectra.[8] Indeed, a lattice temperature rise of $T<20$ K is expected from the deposited energy and the heat capacity of Cu_2O.[20] The establishment of an exciton temperature different from the lattice temperature is understandable since the exciton-exciton scattering time is short, on the order of picoseconds, while the exciton–acoustic-phonon scattering time is on the order of nanoseconds.

The second significant result is that the orthoexciton luminescence does not show a sharp peak as expected for a large condensate fraction; rather the spectrum keeps a nearly *constant shape*, i.e., constant $\alpha=-\mu/k_BT$, as the gas increases in density and temperature. From Eq. (2) this implies that the system moves parallel to the Bose-

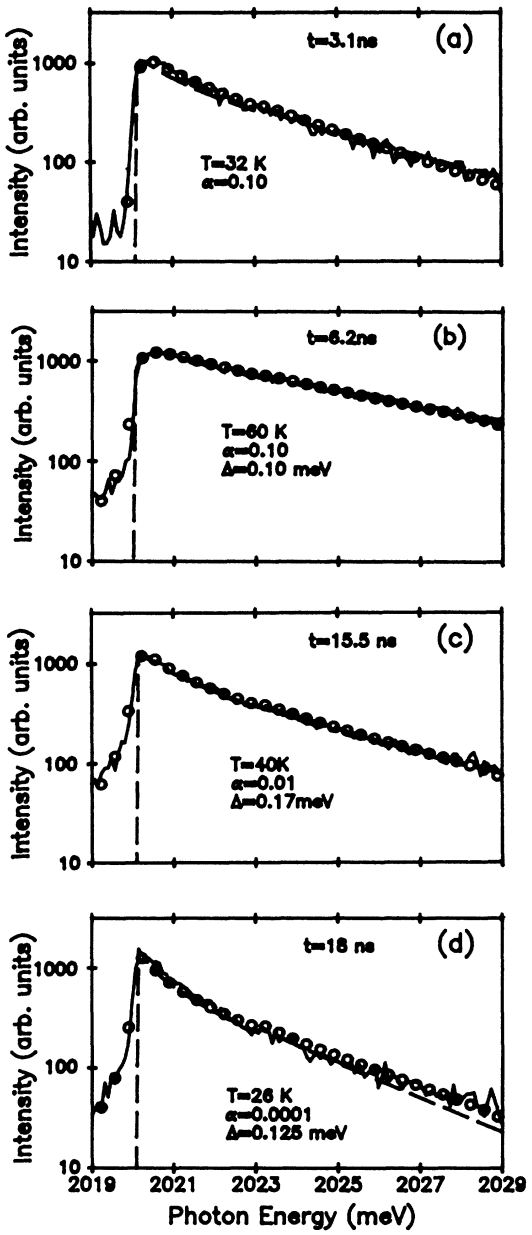

FIG. 4. Several orthoexciton spectra of Fig. 3, plotted logarithmically. (a) Time $t=3.1$ ns. The dashed-line fit to the data is an ideal Bose-Einstein (BE) distribution with $\alpha=0.1$, $T=30$ K. The open circles are a fit to a BE distribution with $\alpha=0.1, T=32$ K convolved with the spectrometer triangle function with FWHM $=0.5$ Å$=0.16$ meV. No Lorentzian spectral broadening is seen. (b) Time $t=6.2$ ns. The dashed-line fit to the data is an ideal BE distribution with $\alpha=0.15$, $T=55$ K, assuming no spectral broadening. The open circles are a fit to an ideal BE distribution with $\alpha=0.1, T=60$ K, convolved with a Lorentzian with FWHM of 0.1 meV. (c) Time $t=15.5$ ns. The dashed line is an ideal BE fit with $\alpha=0.1, T=30$ K, with no spectral broadening. The open circles are a BE distribution with $\alpha=0.01, T=40$ K, convolved with a Lorentzian with FWHM of 0.17 meV. Although the density is lower than in Fig. 4(b), the spectral broadening is greater. (c) $t=18$ ns. The dashed line is a fit to an ideal BE distribution with $\alpha=0.03, T=26$ K with no broadening. The open circles are a fit to a BE distribution of $\alpha=0.0001, T=26$ K, convolved with a Lorentzian with FWHM of 0.125 meV.

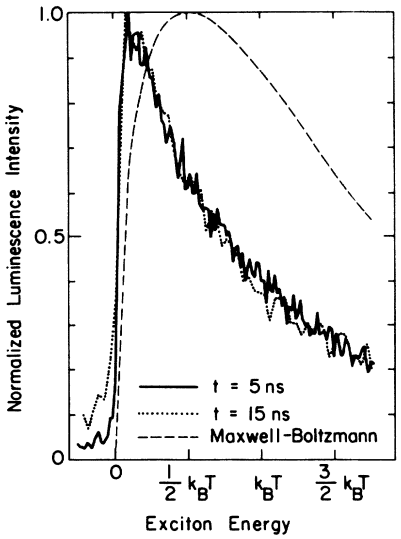

FIG. 5. The quantum "saturation" of the orthoexciton energy distribution. The data of Fig. 3 from two times, at very different temperatures, are plotted on an energy scale normalized by fit temperature. Both curves have the same shape, i.e., the same degeneracy α, which is very different from the classical Maxwell-Boltzmann (MB) distribution.

Einstein phase boundary, $n = CT^{3/2}$. Figure 5 illustrates this shape invariance for two quite different temperatures and densities. One spectrum, taken at $t = 5$ ns, has $n = 2\times10^{19}$ exciton/cm^3, $T = 60$ K; the second spectrum, taken at 15 ns, has $n = 7\times10^{18}$ excitons/cm^3, $T = 30$ K. In this figure, the horizontal energy scale is normalized to the gas temperature in each case.

IV. LOW-ENERGY TAIL AND SPECTRAL BROADENING

An interesting result from the orthoexciton phonon-assisted luminescence is the appearance of the low-energy tail. The width of this tail is significantly greater than the spectral slit resolution. Haug and Kranz[21] have interpreted a similar tail, reported in Ref. 6, as due to interactions with the collective modes of a condensate in a dense Bose gas. The tail may also be due to collision broadening. As shown in Fig. 4, the phonon-assisted luminescence spectra agrees with an ideal Bose-Einstein distribution with a Lorentzian broadening of order 0.1 meV. A Lorentzian shape is predicted by the basic theory of collision broadening.[22] From the uncertainty principle, the width, 0.1 meV, corresponds to a collision time of 12 ps. For particles with a hard-core cross section $\sigma = \pi(7\ \text{Å})^2$, at $T = 30$ K, densities of 10^{18} to 10^{19} excitons/cm^3 give classical scattering times, $\tau = 1/n\sigma v$, from 3 to 30 ps. In this estimate, we have used the excitonic Bohr radius as the representative hard-core radius.

The width of the broadening, however, does not always correlate with the density. In particular, the broadening appears more strongly at late times. For instance, in Fig. 4, the maximum of the density corresponds to the spectrum of Fig. 4(b), which is fit with an energy broadening of 0.1 meV. The maximum of the broadening, however, corresponds to Fig. 4(c), where the density has fallen by a factor of 3 and the broadening width is 0.17 meV.

This behavior is difficult to explain if the low-energy tail is simply due to collision broadening. On the other hand, a tail may also be generated from interactions with condensate collective modes. These should be much stronger than excited-particle interactions due to the coherence of the excitation modes. One can postulate that the late-time spectra include a condensate component that, though small, leads to a large broadening in addition to the collision broadening. Although the fits give values of α slightly different from zero, part of the orthoexciton gas may be condensed but obscured due to spatial integration of luminescence, as discussed in Sec. V. The interaction may also be with a condensate in the paraexciton species, even if the orthoexcitons do not condense.

Another possibility is that a small hot lattice region could explain the late-time appearance of the low-energy tail. Because the phonons emitted by the carriers in the thermalization process take some time to convert to low-energy acoustic phonons, the lattice may have a time lag in its thermal expansion. One can imagine that the volume of the exciton gas includes a small hot spot with red-shifted luminescence spectrum, contributing to a low-energy tail. From the intensity of the tail, the excitons in a hotter region must comprise less than 10% of the total gas.

Additional information concerning the interpretation is obtained from the orthoexciton direct-recombination line. Because no phonons participate in this process, only states with near-zero momentum (i.e., $k \simeq k_{\text{photon}}$) are observed. Figure 6 shows the orthoexciton direct-recombination line at three different times. During the laser pulse, the direct line exhibits a broadening to up to a width of 0.15 meV. This broadening is comparable to that observed for the orthoexciton phonon-assisted line. Its symmetric shape, indicated by the dashed Lorentzian fit, argues for interactions within the gas and is not what

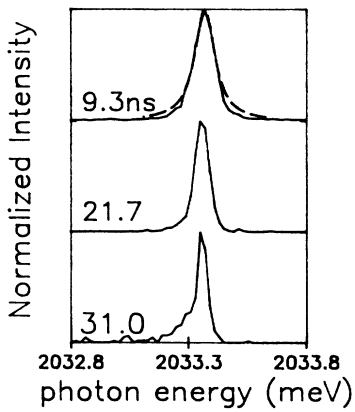

FIG. 6. Orthoexciton direct-recombination luminescence (quadrupole line) under somewhat lower-power conditions than Fig. 3, at three times. The line shows a broadening during the laser pulse consistent with the low-energy tail on the phonon-assisted luminescence. The dashed curve on the early-time data is a fit to a Lorentzian with half width 0.1 meV.

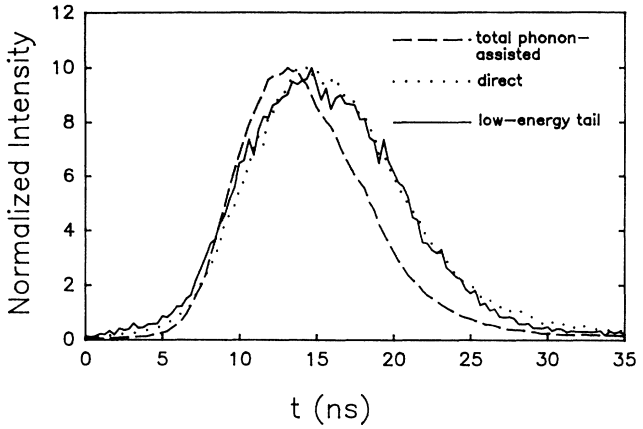

FIG. 7. Dashed curve: The total Γ_3^--phonon-assisted orthoexciton luminescence vs time for the same excitation conditions as the data of Fig. 6. Solid curve: The luminescence of the "low-energy tail" ($E < 2020$ meV) of the phonon-assisted line. Dotted curve: The total orthoexciton direct luminescence vs time. All three curves are normalized to the same height. The low-energy tail and the direct-recombination luminescence show a correlation.

is expected from a small region of red-shifted luminescence. After the laser pulse the direct line narrows to its intrinsic (low-density) width of 0.04 meV. At very late times, a broad red-shifted component of the direct recombination line does appear. Since the gas volume at these times is very large, a red shift may come from impurity-induced band-gap fluctuations in the bulk.

The total integrated signal of the direct line is relatively higher than that of the phonon-assisted line at later times. Figure 7 shows (a) the total (i.e., spectrally integrated) phonon-assisted luminescence intensity, (b) the total direct luminescence, and (c) the total intensity of the "low-energy tail" of the phonon-assisted luminescence for the orthoexcitons as functions of time during the laser pulse. The total intensity of the low-energy tail correlates in time with the direct-recombination line. Since the direct line involves only low-momentum states, it is not surprising that its total intensity shows the same temporal behavior as the low-energy tail. This correlation in time is hard to reconcile with the view of the low-energy tail as due to a region of lattice red shift, since there is no reason for the total direct recombination to be enhanced due to a small hot lattice region. Indeed, the late-time growth of the low-energy tail may be evidence for the collective modes theoretically predicted for a Bose-Einstein condensate.

V. EFFECTS OF SPATIAL INHOMOGENEITIES

Surface excitation produces an excitonic gas that has a range of densities and temperatures. The laser profile is approximately Gaussian, introducing spatial inhomogeneity along the surface. Also, the gas diffuses from the extremely dense region near the surface to zero density deep inside the crystal. Spatial selection of the luminescence over two dimensions is accomplished by the imaging method described above, but spatial integration in the third dimension is unavoidable.

Figure 8(a) shows a simple model of the temperature and density variation as functions of the distance x from the surface, at a given time during the excitation. The local gas density n is assumed to decrease away from the surface with the diffusive form $n = n_{\max}\exp(-x^2)$. Spatial profiles of the luminescence (see Fig. 16) display a distribution qualitatively similar to this at later times in the expansion process. The temperature is assumed to have the form

$$T = T_{\max}\exp(-x^2/1.5) + T_{\text{latt}} ,$$

which gives temperature proportional to $n^{2/3}$ at high densities, in agreement with the observed $n \propto T^{3/2}$ saturation, and falls to the lattice temperature at low densities. Given this form of density and temperature variation, a spatially integrated spectrum is calculated by assuming a

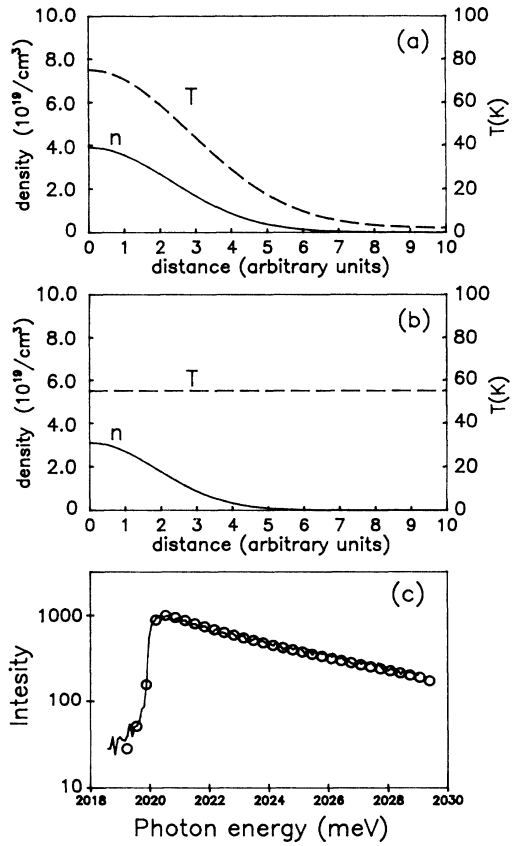

FIG. 8. (a) Model of a possible exciton density and temperature distribution as a function of distance away from the surface. T is proportional to density to the $\frac{2}{3}$ power at high densities, and falls to the lattice temperature of 2 K well inside the crystal. The minimum α is at the surface and equals 0.098, determined by the best fit to spectrum in (c). (b) Another possible exciton density and temperature distribution as a function of distance away from the surface. The minimum α, at maximum density, is found in this case to be 0.025. (c) Solid line: the same data as Fig. 4(c). Open circles: The luminescence spectra from summing a number of local spectra over the distribution of (a), assuming that the spectrum at all densities is a Bose-Einstein distribution. The overall spectrum is convolved with a Lorentzian of half width 0.125 meV.

Bose-Einstein spectrum of the form $D(\epsilon)f(\epsilon,\alpha)$ at each value of x. The fit parameters are now n_{max} and T_{max} instead of n and T as in the previous fits. The circles in Fig. 8(c) show the integrated spectrum calculated from the spatial distribution of Fig. 8(a) and convolved with a Lorentzian broadening of width 0.125 meV. The fit to the data of Fig. 4(b) (solid line) is quite good. In this best fit, the local α increases from 0.098 at the surface to infinity inside the crystal. The temperature at the surface is 75 K.

Figure 8(a) corresponds to the case of zero heat conductivity, with temperature depending only on the local density. Figure 8(b) shows a similar model, but with constant temperature, corresponding to the case of infinite heat conductivity. The true distribution presumably lies between these two extremes. The density variation in Fig. 8(b) has the same form as in Fig. 8(a). In this case the best fit for α_{min} is 0.025, and the temperature is 50 K. The agreement of the spectrum calculated from this model to the data of Fig. 4(c) (not shown because it overlaps the previous fit) is also quite good.

We have also considered a model with density proportional to $x\exp(-x^2)$, possibly corresponding to the case of drift away from the surface or rapid surface recombination. The assumed temperature variation has the form as in Fig. 8(a). Again, using n_{max} and T_{max} as adjustable parameters, a good agreement is obtained with the spectrum.

We conclude that different spatial models give about the same luminescence spectrum as long as they have similar average properties. The n_{max} obtained from fits of these models to the data is about the same as the density obtained from the fit assuming a homogeneous gas. We can therefore use the values for density and temperature obtained from the homogeneous fits with confidence that they represent the average properties of the gas.

VI. HIGHLY DEGENERATE PARAEXCITON LUMINESCENCE

We have concluded above that the orthoexciton gas is either extremely close to condensing or possibly has a small condensed fraction. What about the paraexcitons? One expects that the photoexcitation and thermalization processes create orthoexcitons and paraexcitons in the 3:1 ratio of their spin degeneracy. The paraexciton band lies 12 meV lower and has longer intrinsic lifetime, however, so that down conversion of orthoexcitons quickly produces a gas dominated by paraexcitons. The interconversion rate is known to be a few nanoseconds,[23] which is the principal loss mechanism of the orthoexcitons. Since the paraexcitons have only one spin state instead of three, they may reach higher levels of quantum degeneracy, depending on the speed of the interconversion process compared to the volume expansion rate.

Due to the spin selection rule, the radiative efficiency of the paraexciton phonon-assisted luminescence is less than the main orthoexciton phonon-assisted line by a factor of 1500 ± 300,[24] so that when time-resolved data is taken at roughly equivalent para and ortho densities, the paraexciton luminescence is nearly impossible to see. (Previous studies of paraexcitons have integrated the luminescence over times comparable to their microsecond lifetime. Here we have no such luxury, because the near-critical densities exist only for a few nanoseconds due to the rapid particle diffusion after the laser pulse.) The situation is exacerbated by the close proximity of an orthoexciton phonon-assisted line. However, by integrating over long periods (roughly two hours) with high laser-pulse repetition rate ($\sim$1 MHz), we have been able to observe the paraexciton spectrum during the pulse.

Figure 9 shows the orthoexciton and paraexciton luminescence spectra, taken at the same time during moderate-power laser excitation. The two spectra are normalized in intensity and plotted with the same energy scale. The paraexciton spectrum has had a baseline subtracted. The paraexciton distribution is clearly much narrower than the orthoexciton spectrum, as indicated by their half widths (dotted lines). If we make the reasonable assumption that both species of excitons have the same temperature, as expected in this dense gas with picosecond collision times, then the narrower paraexciton line shape implies that the paraexcitons have greater degeneracy. The orthoexciton line shape yields $\alpha=0.31$ and $T=26$ K at this time. The fit to the paraexciton

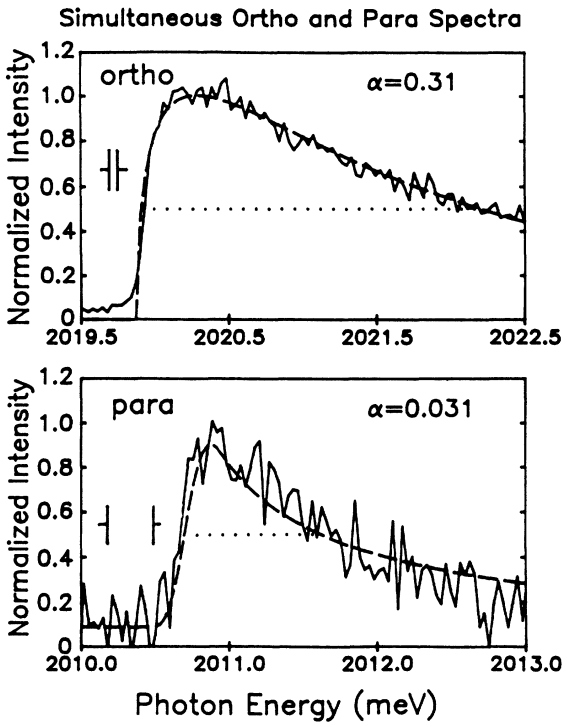

FIG. 9. The orthoexciton (Γ_3^--phonon replica) and paraexciton (Γ_5^- replica) spectra at the same time during a laser pulse with incident power $\simeq 5\times10^6$ W/cm^2, corresponding to the data of Fig. 10(c). The half widths are shown by the dotted lines. The paraexciton luminescence has much smaller half width, indicative of a more degenerate paraexciton distribution. The orthoexciton spectrum is fit to a BE distribution with $\alpha=0.31$ and $T=25$ K, and the paraexciton spectrum is fit to a BE distribution with $\alpha=0.031$ and $T=25$ K.

spectrum in Fig. 9, shown as the dashed line, has been obtained by fixing the temperature to $T=26$ K and varying α. In this case, the paraexciton distribution is best fit by a Bose-Einstein distribution with $\alpha=0.031$.

In addition to fitting the spectral distributions, there is another method of estimating the density of the paraexciton gas. One can deduce the absolute ratio of orthoexcitons to paraexcitons by comparing their total luminescence intensities at the same time. The volumes of the ortho and para components are found to be the same (see below) so that their relative densities may be ascertained. This method relies on a previous calibration of the radiative strengths of the various exciton lines.[8,24]

Figure 10 shows the total Γ_3-phonon-assisted orthoexciton luminescence and the total Γ_5-phonon-assisted paraexciton luminescence as functions of time, for several different excitation-power densities. These data are all taken with approximately the same laser power but differing spot sizes, so the uncertainty in the power density is about a factor of 2. The paraexciton intensity has been multiplied by a factor of 1500 (the relative luminescence strength) and corrected for different spectrometer slit width and integration time. The ratio of ortho and para intensities in this figure therefore corresponds to the ratio of their densities. Notice that in all cases the orthoexciton-to-paraexciton ratio is much greater than expected from a simple Boltzmann population, $\exp(-\Delta/k_BT)\simeq 10^{-15}$ to 10^{-2}. This is due to the density-dependent Auger-like process discussed in the following.

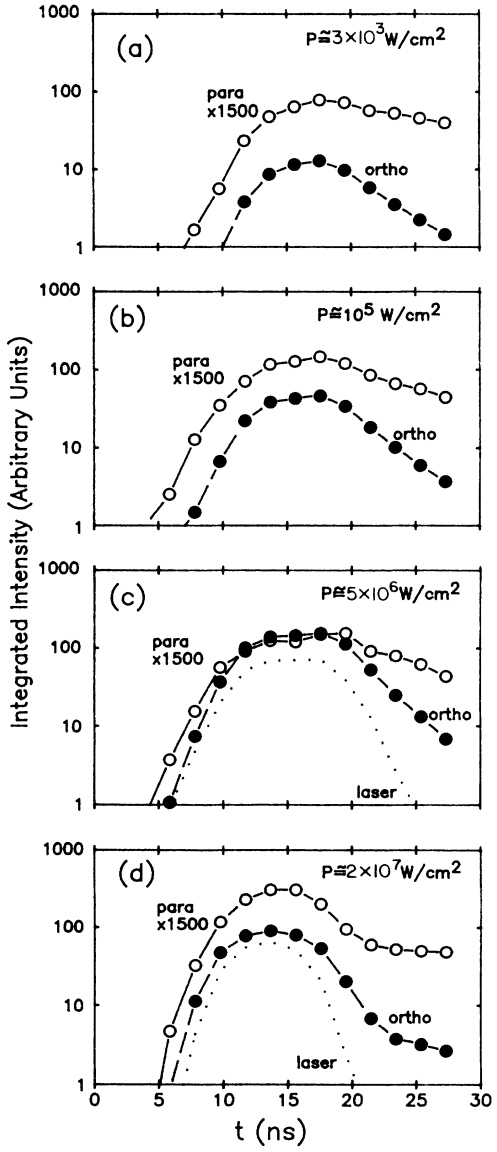

FIG. 10. The relative number of paraexcitons and orthoexcitons during laser pulses at several power levels, based on the total integrated luminescence of the two species. The paraexciton intensity is multiplied by 1500 to indicate the relative densities of the two species. As seen in this figure, the ratio of paraexcitons to orthoexcitons *decreases* as density increases *except* at highest densities, shown in Fig. 10(d).

Figure 11 shows the orthoexciton and paraexciton densities during the peak of the laser pulse for the four laser powers shown in Fig. 10. The orthoexciton densities have been deduced from fits to the phonon-assisted spectra at the peak intensity. For example, the density determined from the orthoexciton spectrum of Fig. 9 corresponds to the point of maximum intensity in Fig. 10(c), and the second-highest power in Fig. 11. The spectra of Fig. 10(a) are nondegenerate so the spectral fit gives only an upper bound on the density. A lower bound on the density is obtained by comparison of the laser excitation power. The paraexciton density in each case is obtained by multiplying the lower bound of the orthoexciton density by the paraexciton-to-orthoexciton intensity ratio shown in Fig. 10.

As seen in Figs. 10(a)–10(c), as the excitation energy density is raised, the paraexciton density decreases rela-

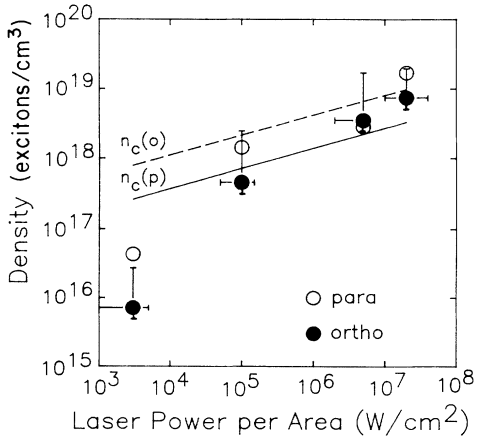

FIG. 11. The maximum density of the orthoexcitons and paraexcitons for the four laser-pulse powers shown in Fig. 10. The orthoexciton density is estimated from the spectral fit at maximum intensity; the paraexciton density is set equal to the orthoexciton density multiplied by the intensity ratio from Fig. 10. The solid and dashed lines indicate the approximate critical densities for the paraexcitons and orthoexcitons, respectively, based on the fit temperature from the orthoexciton spectra. As seen in this figure, the paraexcitons exceed critical density during most of the saturation of the orthoexcitons; at the highest powers, they are nearly an order of magnitude above critical density.

tive to the orthoexciton density. This behavior is expected when Auger nonradiative recombination due to collisions is taken into account. In this process, which has been observed[12,13] to occur in Cu_2O with a cross section of $1-2$ Å^2, two excitons collide and one recombines, giving its energy to ionizing the other. As in the laser-light generation process, the excited electrons and holes reform as excitons with random spin, presumably yielding three orthoexcitons for every paraexciton. At high densities when this process dominates the lifetime, one therefore expects that the orthoexciton density will approach three times the paraexciton density. In the low-to-intermediate-density regime, this model works well; at the highest densities, however, the paraexciton density suddenly increases relative to the orthoexciton density [see Fig. 10(d)], indicating a new channel of orthoexciton-to-paraexciton conversion.

The anomalous rise in the paraexciton population relative to that of the orthoexcitons corresponds to a condition where the paraexciton density greatly exceeds the critical density for condensation. The dashed lines in Fig. 11 give the predicted critical density for the orthoexcitons, as determined from the spectral-fit temperature at each time and Eq. (2). From this equation, the predicted critical densities for paraexcitons at the same time and temperature lie a factor of three *lower* than the dashed curve. As seen in this figure, the paraexciton density exceeds the critical density at all times during the orthoexciton "saturation" just below its critical density. At the highest power density, the paraexciton density exceeds that necessary for condensation by nearly a factor of 5.

We now examine whether there is evidence for a condensed fraction in the paraexciton spectra. Indeed, we find that the paraexciton spectra in this high-density case become anomalous. Figure 12 shows the paraexciton luminescence spectrum as a function of time under high-power excitation conditions ($\sim 5\times 10^7$ W/cm^2), the same data as used in Fig. 10(d). Superposed on the same energy scale is the orthoexciton phonon-assisted luminescence under the same conditions. Because of the high repetition rate, a small amount of excitons from the previous laser pulse are present at the start of the laser pulse. The "$t=0$" spectra show the para and orthoexciton luminescence from the prior pulse. (The paraexciton spectrum at $t=0$ has peak intensity a factor of 4 less than the peak intensity at 3.9 ns, and 50 times less than the maximum intensity at $t=11.7$ ns.) Both the paraexcitons and orthoexcitons have a $T=2.7$ K Maxwell-Boltzmann distribution. As the density increases, the paraexciton line becomes narrower than the orthoexciton line, indicative of higher degeneracy as already discussed. The orthoexciton spectrum is well fit at all times to an ideal Bose-Einstein distribution with rising and falling temperature. At the peak densities, however, the paraexciton spectrum does not fit either a classical or an ideal Bose-Einstein distribution, but instead shows a high-energy bump, or cutoff.

The anomalous bump in the paraexciton distribution could be viewed as a blue-shifted component of the luminescence spectrum. Indeed, Moskalenko *et al.*[25] have predicted a blue shift for the condensed or nearly condensed paraexciton species due to the repulsive interactions of the excitons. The blue shift for paraexcitons is predicted to be much greater than that of the orthoexciton species. Moskalenko *et al.* predict that the blue shift increases linearly with density. The energy position

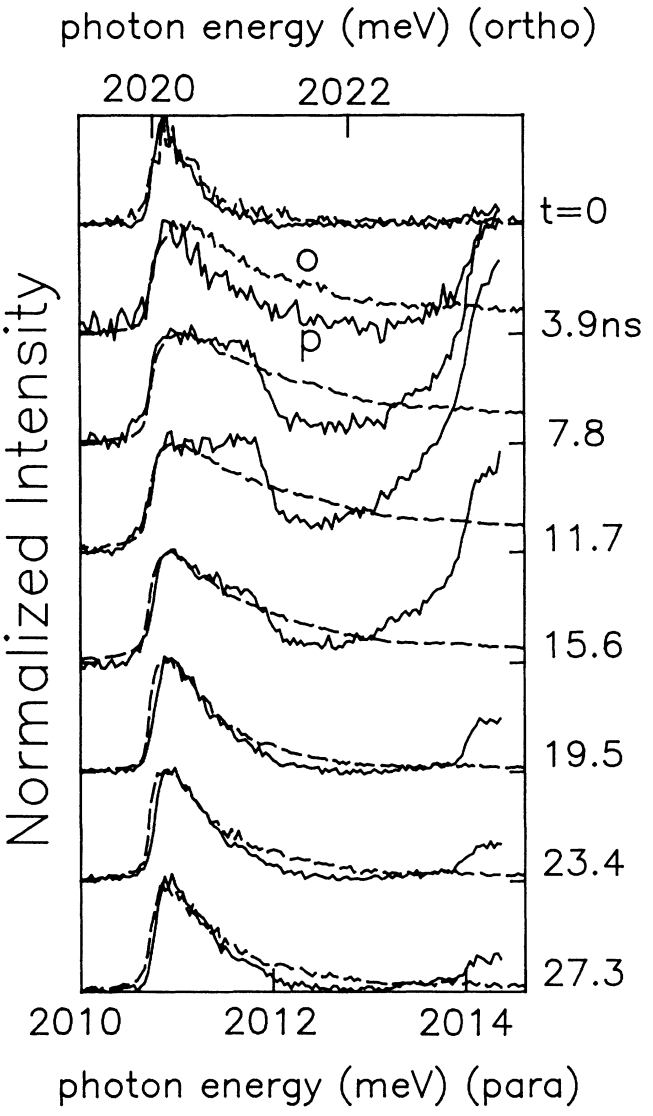

FIG. 12. The spectral data corresponding to Fig. 10(d). Solid curves: the paraexciton phonon-assisted luminescence at various times during and after a cavity-dumped 10-ns Ar^+-laser pulse exciting Cu_2O at 2 K. The spectra show an unusual high-energy bump, or cutoff, during the times of highest density. The large signal at short wavelength is due to the low-energy tail of an orthoexciton phonon-assisted replica. Dashed curves: The orthoexciton phonon-assisted luminescence under the same excitation conditions, normalized to the same height and plotted on the same wavelength scale as the paraexciton luminescence. Both the orthoexciton and the paraexciton spectra fit a Maxwell-Boltzmann distribution with $T=2.7$ K at $t=0$, but they take on very different shapes at later times, until well after the laser pulse.

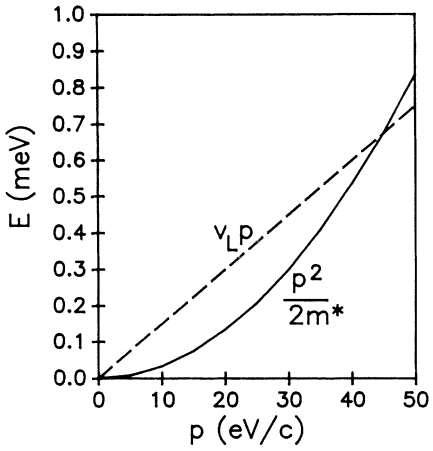

FIG. 13. A possible explanation of the bump in the paraexciton spectra. The dashed line indicates the energy of an exciton which couples directly to the ground state via a longitudinal acoustic phonon.

of the observed bump, however, is relatively independent of time and excitation power.

One may immediately speculate that this highly anomalous energy distribution of the paraexcitons is associated with Bose-Einstein condensation. The additional "bump" in the spectra suggests a condensate into a state with nonzero momentum. Why is the energy fixed at about 1 meV? This energy may be related to the intrinsic energies of the lattice phonons. One possibility involves the longitudinal acoustic phonons in Cu_2O. As shown in Fig. 13, the linear dispersion of the longitudinal acoustic phonons in Cu_2O, $\hbar\omega=\hbar vk$ with $v=4.5\times10^5$ cm/s,[26] crosses the quadratic dispersion of the excitons at an energy of about 0.7 meV. Nonequilibrium phonons flowing from the excitation spot can impart their momentum to the gas, which, if superfluid, would take on a rapid ballistic transport. Due to the linear excitation spectrum at low energies,[27] the superfluid component would not lose this energy rapidly.

An interesting possibility is that the orthoexciton down-conversion process "seeds" the condensed fraction at finite velocity. The upper edge of the bump [i.e., the apparent energy cutoff at 2011.8 meV in Fig. 14(a)] lies 88 cm^{-1} below the ground state of the orthoexcitons, which is the energy of a Γ_5 optical phonon in Cu_2O. This points to the process of the orthoexciton ground state emitting a single 88-cm^{-1} Γ_5 optical phonon to convert to the paraexciton state, as shown in Fig. 15. We can check this possibility by comparing the orthoexciton "ground state" luminescence intensity to the intensity of the paraexciton "bump" luminescence as a function of time. Figure 14(b) shows the laser intensity, the luminescence intensity for the orthoexciton tail and the paraexciton high-energy bump as functions of time. The solid line in Fig. 14(b) gives the time dependence of the intensity of the orthoexciton low-energy tail, shown as the shaded region in the orthoexciton spectrum in Fig. 14(a); the dashed line in Fig. 14(b) gives the intensity of the bump in the paraexci-

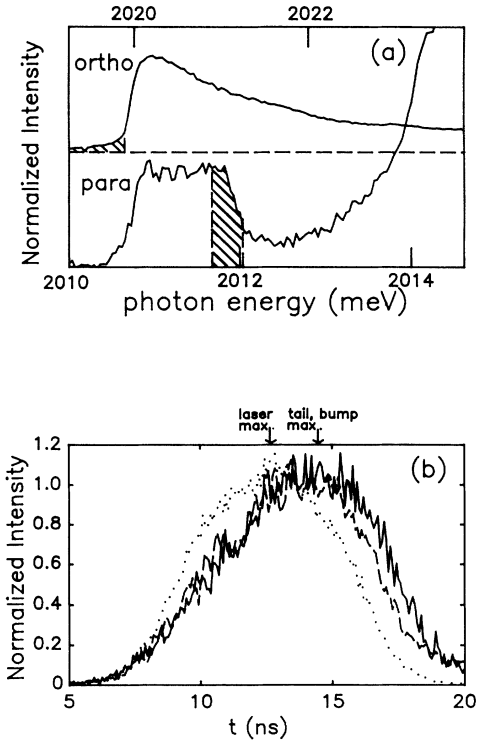

FIG. 14. (a) Orthoexciton and paraexciton spectra from Fig. 12 at $t=11.7$ ns. The time evolution of the shaded regions are compared in part (b), where the solid curve is the luminescence from the orthoexciton low-energy tail [shaded area in the upper spectrum of (a)]. The dashed curve is the luminescence from the paraexciton bump [shaded area in the lower spectrum of (a)] for the data of Fig. 11. Dotted curve: the laser intensity as a function of time during the excitation. The paraexciton high-energy cutoff does not correlate with the laser light but does correlate with the orthoexciton low-energy states.

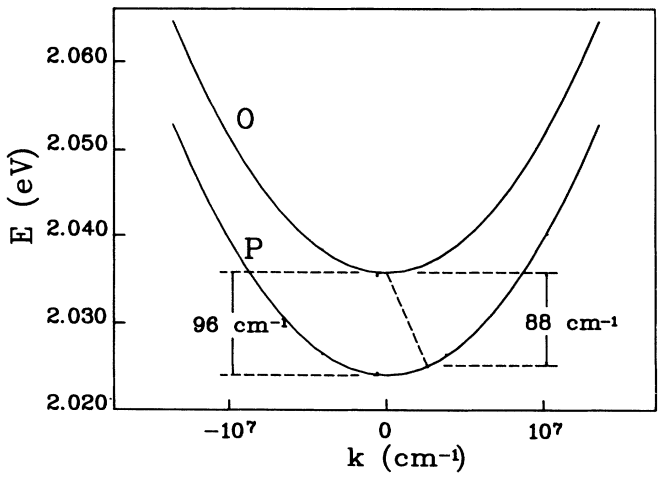

FIG. 15. Possible down-conversion process in Cu_2O: a single 88-cm^{-1} phonon emitted from the zone center of the orthoexciton band. Such a process could "seed" the paraexciton distribution at the 1-meV (8-cm^{-1}) high-energy cutoff in the paraexciton spectrum.

ton spectrum, shaded in the paraexciton spectrum in Fig. 14(a). The dotted line is the laser power versus time. The appearance of the bump in the paraexciton spectrum correlates in time with the ground state orthoexciton luminescence in showing a time lag to its maximum. This gives indirect support to the idea that the paraexciton population is seeded at high density by down conversion from the orthoexciton ground state.

An increased down-conversion rate would help to explain both the saturation of the orthoexciton density at $n_c(T)$ and the rise in the paraexciton-to-orthoexciton ratio at high excitation levels, seen in Fig. 10(d). But why would this Γ_5-phonon down-conversion process be enhanced at high density? One consideration is that the occupation numbers of the paraexciton states are high when the paraexcitons are above the critical density, and any states with occupation number above unity will enhance the interconversion processes into these states. Also, the paraexciton bump may indicate an increase in the population of the orthoexciton ground state; indeed, the orthoexcitons may be partly condensed as indicated by the degenerate fits and the low-energy tail.

The question remains whether the bump at high energy corresponds to a ballistic motion of excitons. As mentioned above, it is expected that a condensate moving at finite velocity will experience greatly reduced scattering with lattice phonons due to the coherent quantum nature of the system, i.e., a superfluid flow of excitons.[10,27,28] With this impetus, we have examined the spatial expansion of the exciton gas as a function of excitation density.

VII. NONDIFFUSIVE EXPANSION OF THE EXCITONIC GAS

As seen in Fig. 11, at high powers the paraexcitons have an average density above the critical density for Bose-Einstein condensation. This is true even well after the laser pulse, since the paraexcitons have much longer lifetime than the orthoexcitons and the temperature is falling quickly. If the paraexcitons are condensed, is there any evidence for superfluid transport? Fast transport rates are predicted for Bose-condensed excitons.[10]

Figure 16 shows the spatial distribution of both the orthoexcitons and paraexcitons, normalized in intensity, at three different times during and after an intense laser pulse. The luminescence in each case is spectrally integrated over a range of 15 Å. The paraexciton spatial distribution has had the broad distribution remaining from the previous laser pulse subtracted. A width Δ is defined for each distribution which is the distance from the surface to the inner half-maximum intensity. In the case of simple diffusion, neglecting surface recombination, the distribution should be Gaussian at all times with half width $\Delta=(2.77Dt)^{1/2}$ where D is the diffusion constant. As seen in this figure, the orthoexcitons and paraexcitons have about the same volume at all times. This does not necessarily mean that the orthoexcitons and paraexcitons have the same diffusion constant. A gas dominated by paraexcitons produces orthoexcitons by the Auger process, so at later times in the expansion process the distribution of orthoexcitons is partly due to a local generation of orthoexcitons within the paraexciton gas.

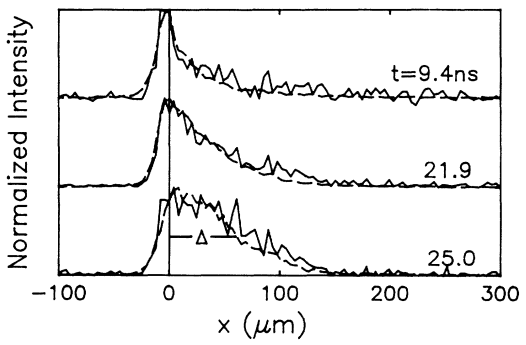

FIG. 16. Solid curves: the paraexciton spatial distribution for three times during and after the laser pulse. The early-time paraexciton distribution, remaining from the previous laser pulse, has been subtracted. $x=0$ corresponds to the crystal surface. Dashed curves: the orthoexciton distribution at the same times.

Figure 17 shows the width Δ of the orthoexciton distribution as a function of time during and after the laser pulse for several laser-power densities. At the lowest observed densities, the behavior is diffusive with diffusion constant about 700 cm^2/s (neglecting the effect of surface recombination, which is discussed in the following). This compares to the measured diffusion constant for paraexcitons of 600 cm^2/s at $T=2$ K.[18] In fact, the lattice temperature determined from the late-time paraexciton spectral distribution is about 4 K, indicating that the photoexcited crystal is hotter than the 2-K bath temperature. The measured D at 4 K is only 200 cm^2/s, and falls roughly as $T^{-1/2}$ at higher temperatures.

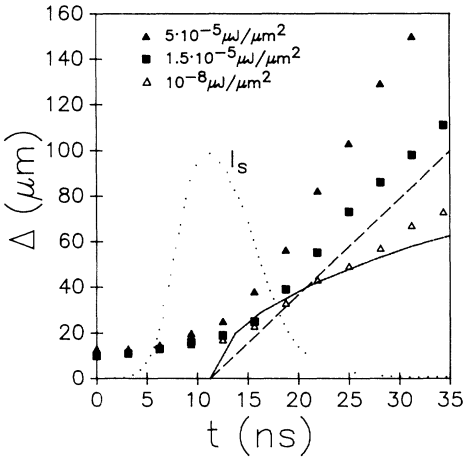

FIG. 17. *Supersonic transport of the excitons at high power.* The distance Δ, measured from the surface to the innermost half maximum of the spatial distribution, for the orthoexcitons as a function of time for several laser-power densities. Open triangles: pulse energy/area $\simeq 10^{-8}$ μJ/μm^2. Solid squares: pulse energy/area $\simeq 1.5\times10^{-5}$ μJ/μm^2. Solid triangles: pulse energy/area $\simeq 5\times10^{-5}$ μJ/μm^2. The dashed line has slope given by the average longitudinal acoustic-phonon velocity in Cu_2O, 4.5×10^5 cm/s. The solid curve is equal to $\sqrt{2.77Dt}$, with $D=600$ cm^2/s, previously measured (Ref. 18) for paraexcitons at $T=2$ K. The dotted line labeled I_s gives the total luminescence at the surface of the crystal as a function of time, which roughly follows the laser intensity.

At high powers, the distribution expands more rapidly, with a ballistic character. For the highest excitation level (15-μm laser spot, 5×10^7 W/cm^2) an expansion velocity of 6.5 μm/ns$=6.5\times10^5$ cm/s is observed. This is faster than the longitudinal acoustic-phonon speed[26] of 4.5 μm/ns. This supersonic velocity is comparable to the group velocity of excitons at the anomalous bump in the paraexciton spectrum, $v_g=10$ μm/ns. An exact equality is not expected, of course, since the spatial distribution has contributions from excitons in excited states as well as those in a condensed fraction. Also, the dispersion relation of the condensed gas may be significantly modified as in Fig. 13. Nevertheless, the observation of a power-dependent ballistic or driftlike motion, which is supersonic at the highest levels, provides a compelling argument for a nonclassical transport.

Nondiffusive motion of excitonic matter has been previously observed[29] for electron-hole liquids in Ge and Si and for free excitons in CdS.[30] In those cases, near-sonic velocities were clearly attributed to drift motions of electron-hole droplets in a "wind" of ballistic phonons. Anisotropic clouds of electron-hole droplets in Ge provided graphic proof of this phonon-wind mechanism.[31] In those experiments, however, the drift was strictly limited to subsonic velocities. Such velocity-saturation behavior (actually at the transverse phonon velocity) has been clearly observed in silicon.[32] Therefore, the supersonic transport velocities observed here for the degenerate excitons in Cu_2O are quite novel, suggesting that the damping of the exciton motion by phonon emission is greatly reduced.

Proper interpretation of the anomalous transport must take into account the lifetimes of the excitons. Recombination at the crystal surface can affect the spatial distribution of the excitonic gas and lead to apparently faster-than-diffusive motion. For example, surface recombination velocities of 2×10^5 cm/s for photoexcited carriers in Si led to driftlike temporal behavior[33,34] with apparent drift velocities of about 2×10^5 cm/s. While some degree of surface recombination is inevitable in the expansion in Cu_2O, this effect cannot explain all of the data. First, the observed expansion at high powers is faster than expected for surface recombination, even in the case of infinite surface-recombination velocity (boundary condition $n=0$ at $x=0$.) In that case, the solution of the diffusion equation by the method of images in one dimension gives the analytic form of the spatial distribution as

$$n \propto x t^{-3/2} \exp(-x^2/4Dt) ,$$

with half width $\Delta=(7.45Dt)^{1/2}$ where D is the diffusion constant. Thus, this extreme case of infinitely fast surface recombination leads to an increase in Δ by $(7.45/2.77)^{1/2}$, or only about 60%. Two other observations argue that surface recombination does not explain the observed rapid expansion: (1) the high-power expansion appears to be linear with time over the observed range, rather than proportional to $t^{1/2}$; (2) the expansion velocities depend on excitation power, and the low-power data shows diffusive expansion with D about equal to that measured for paraexcitons, without recourse to surface recombination effects. At high power, the measured expansion velocities are close to the calculated *ballistic* velocities in the gas.

At this stage, we have considered only some of the simple aspects of the expansion processes. In fact, the temperature of the two-component gas may be inhomogeneous, and this can affect the overall transport, although the gas has cooled significantly at the times when supersonic velocities are observed (e.g., 25 ns in Fig. 17.) Also, the larger densities at the surface lead to shorter lifetimes which will modify the distribution from that expected for simple diffusion or drift. In addition, the orthoexcitons and paraexcitons should have quite different phonon-scattering times.

VIII. SUMMARY AND CONCLUSIONS

In a previous publication, we analyzed the photoluminescence spectra of orthoexcitons with the simple distribution of an ideal Bose gas, given by $f(\epsilon,\alpha)D(\epsilon)$. The analysis showed a quantum saturation of the gas with $\alpha=0.1$ over a wide range of densities. In this paper we have taken into account spectral broadening due to interactions between particles and to spatial inhomogeneities. The occurrence of a low-energy tail in the spectrum at high gas densities is a clear indicator of particle interactions. This feature can be accounted for by incorporating a Lorentzian broadening with a value close to that expected from interparticle collisions. When this interaction broadening is included, the spectral fits yield nearly zero chemical potentials, indicating that at high excitation levels the orthoexciton gas is right at the phase boundary for Bose-Einstein condensation. To determine the effect of spatial inhomogeneities in the gas density and temperature, we have summed local Bose spectra over a range of densities and temperatures. This composite spectrum fits the experimental spectrum well and indicates that the region of maximum gas density is very close to condensation. At high excitation, the orthoexciton gas seems to be pinned at the phase boundary.

Given this quantum saturation of the orthoexcitions, we have observed the much weaker photoluminescence of the lower-lying paraexcitons. At intermediate excitation levels, the paraexciton distribution is narrower than the corresponding orthoexciton distribution, indicating that the paraexcitons are more degenerate. This observation is not surprising, considering the three-times-smaller spin multiplicity of the paraexcitons and their rapid generation by down-conversion of orthoexcitons. Indeed, a determination of the relative intensities of orthoexcitons and paraexcitons indicates that the paraexciton gas reaches or exceeds its critical density at these excitation levels. As the excitation level is raised further, the paraexciton spectrum exhibits an anomalous non-ideal-gas shape. A distinct spectral bump, or cutoff, is observed at about 1 meV above zero kinetic energy. At these high excitation levels, the total intensity of the paraexciton luminescence increases relative to the orthoexcitons. The position of the spectral bump in the paraexciton spectrum suggests a couple of interpreta-

tions. It is separated from the bottom (zero kinetic energy) of the Γ_5-orthoexciton replica by the energy of a Γ_5 optical phonon, suggesting that the paraexciton gas is "seeded" by interconversion of orthoexcitons with the emission of this optical phonon. The enhancement of this process at high particle densities may be caused by an increased population of the zero-energy orthoexcitons (i.e., due to condensation) and the degenerate final-state population of excitons.

A second consideration is that the paraexciton bump appears close to the energy where the longitudinal acoustic-phonon dispersion crosses the single-particle exciton dispersion curve. This suggests that absorption of acoustic phonons leaving the excitation region may cause the paraexcitons to form a condensate with nonzero momentum.

Evidence for ballistic propagation is found in the time-resolved spatial profiles of the exciton gas. In contrast to classical diffusion, the expansion rate is found to increase with excitation level, and at the highest powers the expansion velocity is close to the ballistic velocity of excitons with 1-meV kinetic energy. The observed expansion rate greatly exceeds that expected for diffusion, even at the large diffusion constant previously measured for paraexcitons at low gas densities. Of course, this is hardly a simple diffusion process described solely by exciton-phonon collisions, as in the low-density case. At high densities the particle lifetimes are density dependent, which can alter the spatial distributions. And, at least during the excitation pulse, the gas temperature and the lattice temperature are significantly different. Nevertheless, these first experiments show a nondiffusive transport of the exciton gas at near-ballistic velocities, which, together with the time-resolved spectral information, provide a compelling case for Bose-Einstein condensation and excitonic superfluidity.

One of the most interesting theoretical aspects of this system is the role of interactions in the condensation process. Aside from the simple collisional broadening, we have ignored the presence of interactions in the spectral analysis. At the highest experimental densities, the exciton gas is approaching the region where it may not be considered an ideal gas. As previously mentioned, $na^3=0.04$ for $n=10^{20}/\text{cm}^3$ and $a=7$ Å, and the interaction energies should be a few Kelvin in this density range. The thermodynamics of the quantum exciton gas (e.g., heat capacity and the nature of the phase transition) remains as an intriguing problem.

ACKNOWLEDGMENTS

This work was supported by National Science Foundation Grant No. DMR87-22761. Facility support was provided by the National Science Foundation under the Materials Laboratory Grant No. DMR86-12860. We acknowledge the U.S. Air Force Office of Scientific Research (AFOSR) and NATO (travel grant) for earlier support of this work. Natural Cu_2O samples were obtained by a gift from P. J. Dunn of the Smithsonian Institute. We thank A. Griffin, P. Nozieres, and M. Tamor for helpful conversations. Laboratoire d'Optique Appliquée and Groupe de Physique des Solides are each Laboratoire associé au Centre National de la Recherche Scientifique (CNRS).

[1]Early predictions of excitonic Bose-Einstein condensation were made by S. A. Moskalenko, Fiz. Tverd. Tela **4**, 276 (1962); I. M. Blatt, K. W. Boer, and W. Blatt, Phys. Rev. **126**, 1691 (1962); and R. C. Casella, J. Phys. Chem. Solids **24**, 19 (1963).

[2]For theory of excitonic Bose-Einstein condensation, see E. Hanamura and H. Haug, Phys. Rep. **33**, 209 (1977); C. Comte and P. Nozieres, J. Phys. (Paris) **43**, 1069 (1982); **43**, 1083 (1982).

[3]A review of experimental work in excitonic Bose-Einstein condensation is given by A. Mysyrowicz, J. Phys. (Paris) **41**, Suppl. 7, 281 (1980).

[4]V. B. Timofeev *et al.*, in *Proceedings of the Sixteenth International Conference on Physics of Semiconductors, Montpellier, France, 1982,* edited by M. Averous (North-Holland, Amsterdam, 1983), p. 327.

[5]N. Peghambarian, L. L. Chase, and A. Mysyrowicz, Phys. Rev. B **27**, 2325 (1983).

[6]D. Hulin, A. Mysyrowicz, and C. Benoit a la Guillaume, Phys. Rev. Lett. **45**, 1970 (1980).

[7]D. Snoke, J. P. Wolfe, and A. Mysyrowicz, Phys. Rev. Lett. **59**, 827 (1987).

[8]A. Mysyrowicz, D. Hulin, and A. Antonetti, Phys. Rev. Lett. **43**, 1123 (1979); **43**, 1275E(E) (1979).

[9]F. Bassani and M. Rovere, Solid State Commun. **19**, 887 (1976), predict that biexcitons do not exist in Cu_2O. A. I. Bobrysheva and S. A. Moskalenko, Phys. Status Solidi (B) **119**, 141 (1983), calculate that the interaction is repulsive in general except between two orthoexcitons with summed spin $S=0$, which can form a biexciton with binding energy ~ 0.7 meV.

[10]V. A. Gergel, R. F. Kazarinov, and R. A. Suris, Zh. Eksp. Teor. Fiz. **54**, 87 (1968) [Sov. Phys.—JETP **27**, 159 (1968)].

[11]D. W. Snoke and J. P. Wolfe, Phys. Rev. B **39**, 4030 (1988).

[12]A. Mysyrowicz, D. Hulin, and C. Benoit a la Guillaume, J. Lumin. **24&25**, 629 (1981).

[13]D. P. Trauernicht, J. P. Wolfe, and A. Mysyrowicz, Phys. Rev. B **34**, 2561 (1986).

[14]I. Pastrnyak, Phys. Status Solidi **1**, 888 (1959).

[15]For a review of carrier-phonon-emission processes see S. E. Esipov and Y. B. Levinson, Adv. Phys. **36**, 331 (1987).

[16]The Bohr radius a of the exciton is estimated from the known binding energy, $E_0=150$ meV, using the hydrogenic relation $E_0=e^2/2\epsilon_0 a$, where ϵ_0 is the dielectric constant.

[17]For a review of Cu_2O properties see V. T. Agekyan, Phys. Status Solidi A **43**, 11 (1977). We use here the O_h symmetry notation given by Γ_1, Γ_2, Γ_3, Γ_4, and Γ_5, equivalent to Γ_1, Γ_2, Γ_{12}, Γ_{15}, and Γ_{25}, respectively.

[18]D. P. Trauernicht, J. P. Wolfe, and A. Mysyrowicz, Phys. Rev. Lett. **52**, 855 (1984); D. P. Trauernicht and J. P. Wolfe, Phys. Rev. B **33**, 8506 (1986).

[19]Technically, α can never reach exactly zero since this would imply an infinite population of the ground state. In a finite system the proximity of α to zero determines the ground-state population which must be added to the right side of Eq. (2). See C. Kittel and H. Kroemer, *Thermal Physics* (W. H. Free-

man, San Francisco, 1980), p. 205.

[20]The absorbed 0.27-μJ Ar^+-laser energy per pulse corresponds to 7×10^{11} phonons, each with 0.375-eV excess energy, resulting in about 10^{-8} cal delivered to the lattice. For the heat capacity of Cu_2O, roughly 1.4×10^{-6} cal/g K $(T/K)^3$ at low temperature reported by L. V. Gregor, J. Phys. Chem. **66**, 1645 (1962), and the volume of the excitation region of about 2×10^{-8} cm^3, this yields a lattice temperature of 20 K, assuming no lattice energy diffuses from the excitation region. Diffusion of the lattice phonons will reduce this temperature.

[21]H. Haug and H. H. Kranz, Z. Phys. B **53**, 153 (1983).

[22]R. G. Breene, *The Shift and Shape of Spectral Lines* (Pergamon, New York, 1961), p. 221.

[23]J. S. Weiner, N. Caswell, P. Y. Yu, and A. Mysyrowicz, Solid State Commun. **46**, 105 (1983).

[24]The probability of an optical transition to the ground state with participation of the same Γ_5 optical phonon is a factor of 50 ± 2 times larger for the orthoexciton than for the paraexciton, as indicated by absorption measurements by P. D. Bloch and C. Schwab, Phys. Rev. Lett. **41**, 514 (1978). The ratio of the intensity of the ortho Γ_3 phonon-assisted recombination line to the intensity of the Γ_5 phonon-assisted line is 30 ± 5 from our luminescence measurements. Therefore the ratio of the Γ_3 phonon-assisted orthoexciton line to the Γ_5 phonon-assisted paraexciton line is 1500 ± 300.

[25]S. A. Moskalenko, A. I. Bobrysheva, S. S. Russu, V. V. Balgata, and A. V. Lelyakov, J. Phys. **18**, 989 (1985).

[26]J. Berger, J. Castaing, and M. Fischer, J. Phys. (Paris) **40**, Suppl. 11, 13 (1979); J. Hallberg and R. C. Hanson, Phys. Status Solidi **42**, 305 (1970).

[27]It is well known that the low-energy excitations have linear dispersion $E=v_Bp$, where the Bogoliubov velocity v_B depends on the number of particles in the ground state as $\sqrt{N_0}$. An interesting property of a superfluid, which may be relevant here, is the prediction of a maximum velocity $v_B<v_{cr}$, where v_{cr} is the Landau critical velocity. N. Bogoliubov, J. Phys. (Moscow) **11**, 23 (1947); see also A. L. Fetter and J. D. Walecka, *Quantum Theory of Many-Particle Systems* (McGraw-Hill, San Francisco, 1971).

[28]L. D. Landau and E. M. Lifschitz, *Statistical Physics* (Pergamon, New York, 1958).

[29]For reviews of phonon wind effects, see J. P. Wolfe, J. Lumin. **30**, 82 (1985); L. V. Keldysh and N. N. Sibeldin, in *Nonequilibrium Phonons in Nonmetallic Crystals*, edited by W. Eisenmenger and A. A. Kaplyanskii (Elsevier, New York, 1986), Chap. 9.

[30]N. N. Zinov'ev, L. P. Ivanov, V. I. Kozub, and I. D. Yaroshetshii, Zh. Eksp. Teor. Fiz. **84**, 1761 (1983) [Sov. Phys.—JETP **57**, 1027 (1983)].

[31]M. Greenstein and J. P. Wolfe, Phys. Rev. Lett. **41**, 715 (1978); Phys. Rev. B **24**, 3318 (1981).

[32]F. M. Steranka and J. P. Wolfe, Phys. Rev. B **34**, 1014 (1986).

[33]B. Laurich, H. Hilmer, and A. Forschel, J. Appl. Phys. **61**, 1480 (1987); G. Mahler, T. Kahn, A. Forchel, and H. Hilmer, *Optical Nonlinearities and Instabilities in Semiconductors*, edited by H. Haug (Academic, New York, 1987), p. 1986.

[34]M. A. Tamor and J. P. Wolfe, Phys. Rev. B **37**, (1988).